Available online at www.sciencedirect.com
SCIENCE DIRECT®
Carbon 43 (2005) 2379–2388
CARBON
www.elsevier.com/locate/carbon

Adsorption equilibrium of organic vapors on single-walled carbon nanotubes

Sandeep Agnihotri [a], Mark J. Rood [a,*], Massoud Rostam-Abadi [a,b,*]

[a] Department of Civil and Environmental Engineering, University of Illinois, Urbana-Champaign, 205 N. Mathews Ave., Urbana, IL 61801-2352, USA
[b] Illinois State Geological Survey, 605 E Peabody Dr., Champaign, IL 61820, USA

Received 25 October 2004; accepted 19 April 2005
Available online 28 June 2005

Abstract

Gravimetric techniques were employed to determine the adsorption capacities of commercially available purified electric arc and HiPco single-walled carbon nanotubes (SWNTs) for organic compounds (toluene, methyl ethyl ketone (MEK), hexane and cyclohexane) at relative pressures, p/p_0, ranging from 1×10^{-4} to 0.95 and at isothermal conditions of 25, 37 and 50 °C. The isotherms displayed both type I and type II characteristics. Adsorption isotherm modeling showed that SWNTs are heterogeneous adsorbents, and the Freundlich equation best describes the interaction between organic molecules and SWNTs. The heats of adsorption were 1–4 times the heats of vaporization, which is typical for physical adsorption of organic vapors on porous carbons.

Keywords: Carbon nanotubes; Adsorption; Organic

1. Introduction

Adsorption-related applications of carbon nanotubes, in particular single-walled carbon nanotubes (SWNTs), depend on the availability of their internal pore volume that can be varied by subjecting them to different heat treatment processes that open their ends [1] and remove functional groups that block pore entry [2]. Purity of SWNTs is another important factor that influences the overall adsorptivity of a sample. This is because nanotubes are often found mixed with impurities such as carbon coated catalyst particles, graphitic carbons, soot and other forms of carbon that are unavoidable byproducts of the synthesis processes [3]. These impurities could also be highly adsorbent materials and ignoring their presence could grossly misrepresent the adsorption properties of nanotubes.

Adsorption studies of nanotubes are fairly recent. Researchers have reported a wide range of adsorption surface areas (150–3000 m^2/g) for nanotubes [4–6], which are comparable to carbon-based adsorbents that are used for commercial applications. Studies have also shown that carbon nanotubes could efficiently remove trace concentrations of toxic air pollutants [7], have fast adsorption kinetics for removal of contaminants, such as 1,2-dichlorobenzene [8] and fluoride [9] present in water, have modest H_2 storage capacities (~4.2 wt.%) at room temperature [10], and could also be used as sensors for detecting CO, CO_2 [11], and NO_2 and NH_3 [12]. However, only a limited number of theoretical and experimental studies have focused on adsorption of organic molecules on carbon nanotubes. Theoretical

* Corresponding authors. Tel.: +1 217 333 6963; fax: +1 217 333 6968 (M. Rood), tel.: +1 217 244 4977; fax: +1 217 333 8566 (M. Rostam-Abadi).
E-mail addresses: sagnihot@uiuc.edu (S. Agnihotri), mrood@uiuc.edu (M.J. Rood), massoud@isgs.uiuc.edu (M. Rostam-Abadi).

0008-6223/$ - see front matter © 2005 Elsevier Ltd. All rights reserved.
doi:10.1016/j.carbon.2005.04.020

studies have explored interactions of small organic molecules (such as CH_4) with carbon nanotubes [6,13–15] and have reported mechanisms for separation of binary mixtures of other simple alkanes by diffusive flow through nanotubes [16]. A few experimental studies have described adsorption isotherms for benzene, methanol [17] and methane [18], high affinity of nanotubes for ppb levels of dioxins [7], and adsorption kinetics of ethanol, iso-propanol, cyclohexane, benzene and hexane on a variety of HiPco SWNT samples [19]. Most of these studies were performed on nanotube samples that contained uncharacterized amounts of impurities, which may have impacted the intrinsic physical interactions of organic molecules and carbon nanotubes. Therefore, experimental studies involving select organic molecules and well characterized carbon nanotube samples will contribute to the current state of knowledge about adsorption mechanisms of organic molecules on carbon nanotubes.

In this study we gravimetrically measure the equilibrium adsorption capacities of toluene, methyl ethyl ketone (MEK), hexane and cyclohexane vapors on commercially available purified SWNT samples that differed in purity and synthesis method. The adsorbates were carefully chosen to have similar heats of vaporization (i.e. comparable heats of adsorption) but varying dipole moments and structures (Table 1). The adsorption experiments measured SWNTs' capacities for organic molecules at relative pressures, p/p_0, where p is the actual vapor pressure and p_0 is the saturation pressure of the organic vapor, between 1×10^{-4} and 0.95 and at 25, 37 and 50 °C.

Table 1
Physical properties of adsorbates used in this research

Characteristic	Toluene	MEK	Hexane	Cyclohexane
Class	Aromatic	Ketone	Alkane	Cyclic
Molecular formula	C_7H_8	C_4H_8O	C_6H_{14}	C_6H_{12}
Molecular weight (g/mol)	92.15	72.11	86.18	84.16
Heat of vaporization (kJ/mol)[a]	39.2	34.1	31.9	37.7
Dipole moment ($\times 10^{-29}$ C m)[b]	0.13	1.1	0	0.1
Molecular diameter (nm)[c]	0.476	0.275	0.265	0.429
Molecular length (nm)[c]	0.568	0.484	0.681	0.429
Bulk liquid density (cm^3/g) at 25 °C[a]	0.867	0.805	0.66	0.778
Saturation vapor pressure (atm) at 25 °C[b]	0.037	0.118	0.198	0.128
Boiling point (°C)[a]	110.6	79.6	68.8	80.7

[a] *Source*: Ref. [20].
[b] *Source*: Ref. [21].
[c] *Source*: Ref. [22].

2. Experimental

2.1. Sample description

The samples tested in this study were commercially available purified SWNTs that were manufactured by the electric arc (EA) and the HiPco chemical vapor deposition (CVD) [23,24] processes. This combination of samples was selected to provide a range of results that could arise due to the different morphologies of nanotubes generated by the highly energy intensive electric arc method and the low-energy consuming HiPco process [3]. Sample descriptions, morphologies and characterizations are provided elsewhere [25], but brief descriptions of these results are presented here for clarity.

The electric arc sample was purchased from MER Corporation, Tucson, AZ. This sample contained 95–98 wt.% SWNTs (EA95). The residual contamination consisted of <0.5 wt.% Ni/Co catalyst and <5 wt.% of amorphous and graphitic carbons (personal communication with the manufacturer). The sample was produced in November 2001 by purification of the as-produced nanotubes that originally contained 10–15 wt.% SWNTs. Details of how the samples were purified are available elsewhere [26], but are briefly described here for clarity. The manufacturer purified the sample by initially refluxing the as-produced nanotubes for 45 h in a 2–3 M nitric acid. The solution was then centrifuged to yield a black residue of nanotubes. The residue was then washed 3–4 times in deionized water and re-centrifuged to remove the acid trapped in the sediment. The solution pH was then raised to 11 and hollow-fiber cross-flow filtration (CFF) was used to extract SWNTs.

The HiPco sample was purchased from Carbon Nanotechnologies Inc., Houston, TX. The sample contained ≈80 wt.% SWNTs (CVD80), 12 wt.% Fe catalyst and some amorphous and graphitic carbon, as specified by the manufacturer. This sample was produced in November 2002 and was purified by the manufacturer using the same method as described above [26].

The diameters of nanotubes in samples EA95 and CVD80 were determined by Raman scattering ($\lambda = 785$ nm). Majority of nanotubes in sample EA95 were 1.52 nm wide (other sizes: 1.11 and 1.4 nm). On the other hand, most nanotubes in sample CVD80 were 0.9 nm in diameter (other sizes: 1.02, 1.07, 1.15 and 1.18 nm). Therefore, the samples had fundamental difference in morphologies of nanotubes that is expected to influence their adsorption behavior.

The samples were also analyzed to determine the fraction of open-ended nanotubes. This was done by developing a novel methodology that combined molecular simulations of nitrogen adsorption in homogeneous SWNT bundles with standard nitrogen adsorption (77 K) and Raman scattering of samples [27]. It was

Table 2
Physical characteristics of SWNT samples studied

Adsorbent	Total surface area (m^2/g)	External surface area (m^2/g)	Total pore volume (cm^3/g)	Micropore volume (cm^3/g)	Average pore width (nm)
EA95	500	155	0.57	0.16	2.86
CVD80	609	339	0.92	0.07	4.30

Source: Ref. [27].

found that sample EA95 and CVD80, respectively, contained only 45% and 60% open nanotubes. This result is significant as it shows that the adsorption capacities of the two samples could be more than those reported here.

Samples EA95 and CVD80 exhibited "aging", i.e. their nitrogen BET surface areas and pore volumes were observed to change over a period of several months from the time of sample manufacture [25]. Therefore, the organic vapor adsorption study was performed after "aging" had stabilized (7 months < sample age < 16 - months). The adsorption surface areas and pore volumes of the two samples are provided in Table 2.

2.2. Adsorption of organic vapors

2.2.1. Experimental apparatus

The experimental apparatus used to measure the adsorption isotherms consisted of a gravimetric balance (Cahn Model C-2000), a gas generation system and a data acquisition system (Fig. 1). The system was operated in a controlled temperature (25 ± 0.5 °C) and controlled relative humidity (50 ± 1%) room. The limit of detection (LOD) of the balance was measured to be 2 μg. The gas generation system consisted of ultra high purity nitrogen (99.999% pure UHP N_2) as carrier gas in which organic liquid (>99.5% pure) was injected using a syringe pump (K.D. Scientific) and a hypodermic needle. The carrier gas was initially passed through a gas drier/purifier (containing anhydrous $CaSO_4$) to remove any contaminants. Mass flow controllers (Tylan, Models No. FC-280 and FC-260 and Tylan RO-28) were used to control the gas flow rates into the gravimetric balance. The temperature of the sample chamber was controlled with electrical heating tape and a Variac (Staco Energy Products, Type 3PN1010). The sample temperature was measured by a thermocouple placed as close to the sample holder as possible. The data acquisition system gathered mass, time and temperature data every 10 s during a test.

2.2.2. Methodology

Prior to each test, the desired UHP N_2 flow rate was established in the gravimetric balance. The gravimetric balance was then zeroed and calibrated. The adsorbate sample (2–3 mg) was then placed on a sample pan and its initial weight was measured. The sample was heated to 140 °C in UHP N_2 for up to 3 h to desorb volatile materials (mainly H_2O) that were physically adsorbed during storage. The sample was cooled to room temperature and its dry weight was recorded. Desired concentrations of adsorbates were determined by adjusting the flow rate of adsorbate with the syringe pump while

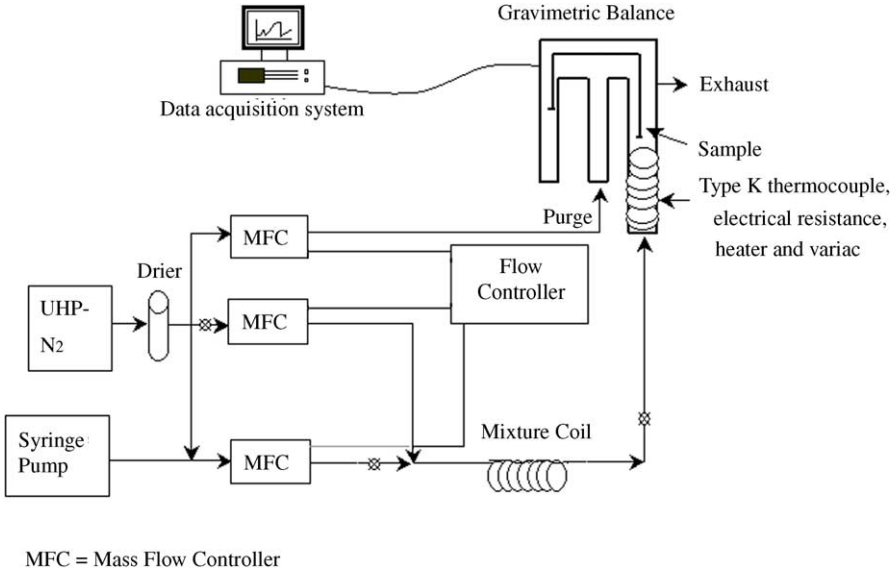

Fig. 1. Schematic of experimental set-up.

keeping the carrier gas flow rate constant. Vapors of known concentrations were then continuously passed through the sample chamber. The sample sorbed vapors and gained mass until equilibrium was achieved. Adsorption equilibrium was assumed to exist when no increase in mass (<2 μg) was observed for 30 min. The gain in sample mass was recorded and the mass ratio of the adsorbed material to the initial mass of adsorbent was reported as the adsorption capacity at the specified vapor concentration. The vapor concentration was then changed by readjusting the liquid flow rate controlled by the syringe pump to obtain another data point. The experiments were performed at ambient pressure at 25, 37 and 50 °C and at vapor concentrations ranging from 40 to 40,000 ppmv ($1 \times 10^{-4} < p/p_0 < 0.95$).

3. Results and discussion

3.1. Adsorption isotherms

The isotherms for toluene, MEK, hexane and cyclohexane adsorption on samples EA95 and CVD80 showed a steep rise below 100 ppmv ($p/p_0 < 10^{-3}$) followed by a slow and steady increase with increasing vapor concentration (Fig. 2). This behavior is typical for a type I adsorption isotherm [28], which is interesting because type I isotherms describe monolayer adsorption mechanisms exhibited by microporous adsorbents [29]. Samples EA95 and CVD80, on the other hand, were mainly mesoporous with only 10–40% of total pore volume in micropores (Table 2). However, unlike most type I isotherms, the adsorption capacities never reached a constant value with increasing vapor concentration but rather continued to increase monotonically until near saturation ($p/p_0 = 0.95$, Fig. 3). This behavior is similar to that of a type II isotherm for mesoporous solids [28]; although, a sharp increase in adsorption near saturation (which is typical of type II isotherms) was not observed in our samples. Therefore, organic vapor adsorption in the tested samples appeared to follow characteristics of both, type I and type II isotherms.

The adsorption capacities of sample CVD80 for all organic vapors at concentrations <1000 ppmv ($p/p_0 < 10^{-2}$) were less than or equivalent to the corresponding values for sample EA95. Thereafter, sample CVD80 exhibited higher adsorption capacities than sample EA95 (Fig. 3). This behavior can be explained as follows. Adsorption on SWNTs is a combination of adsorption [i] in the hollow space inside nanotubes, [ii] in the interstitial spacing between three or more neighboring nanotubes, [iii] on the grooves present on the periphery of a nanotube bundle, and [iv] on the curved surface on the periphery of a bundle [25] (Fig. 4a). Molecular simulations of nitrogen adsorption on arrays of SWNTs of diameters same as those in samples EA95 and CVD80 [27] were used to interpret which adsorption sites were filled with increasing values of p/p_0. The simulations showed that as relative pressure increased until 10^{-2}, the nitrogen molecules completely saturated adsorption sites [i], [ii] and [iii] and formed a monolayer on site [iv]; the total adsorption capacity was dominated by adsorption in site [i] only. However, increasing p/p_0 values above 10^{-2} facilitated only multilayer adsorption on site [iv] at a rate directly proportional to the external surface area of the samples. The simulations also demonstrated that samples composed mostly of narrow nanotubes will have less internal (site [i] + site [ii]) and more external (site [iii] + site [iv]) adsorption than those comprising large diameter nanotubes [27]. Assuming organic vapor adsorption mechanisms follow trends similar to those for nitrogen would mean that until $p/p_0 \leqslant 10^{-2}$ adsorption would mainly occur inside the nanotubes. At $p/p_0 > 10^{-2}$ organic vapor adsorption occurs entirely on the external surface of the bundles, which happens to be the void space between SWNT bundles (Fig. 4b). The trend in adsorption capacities of the two samples, therefore, is a result of sample CVD80 having narrower nanotubes with smaller micropore volume and higher external surface area (Table 2) than sample EA95, which caused less adsorption at $p/p_0 \leqslant 10^{-2}$ but enhanced adsorption at $p/p_0 > 10^{-2}$.

The general trend of organic vapor adsorption capacities of both SWNT samples was toluene (highest) > MEK > hexane > cyclohexane (lowest), which did not seem to follow any particular molecular property (Table 1). Moreover, it was interesting to note that even though toluene and cyclohexane molecules have comparable sizes and equivalent dipole moments, their adsorption capacities differed considerably. For example, at 25 °C and 3500 ppmv concentration the adsorption capacity of sample EA95 for toluene was 33% greater than that for cyclohexane. Increasing the temperature decreased the adsorption capacities of all organic vapors, which indicated exothermic physisorption on nanotubes.

3.2. Maximum adsorption capacities

The maximum organic vapor adsorption capacities and the corresponding pore volumes ($p/p_0 \approx 0.9$) of sample CVD80 were larger than those of sample EA95 (Table 3). This trend was similar to that observed from N_2 adsorption (Table 2). Also, for both samples the total pore volume measured by organic vapor adsorption (Table 3) was 40–50% of the total N_2 adsorption pore volume (Table 2), which is an important observation because the total pore volume is a structural property of an adsorbent which should be insensitive to the adsorbate vapor used for its measurement. The reason for this discrepancy is unknown, although it is believed to be related to the mesoporosity of SWNTs (site [iv],

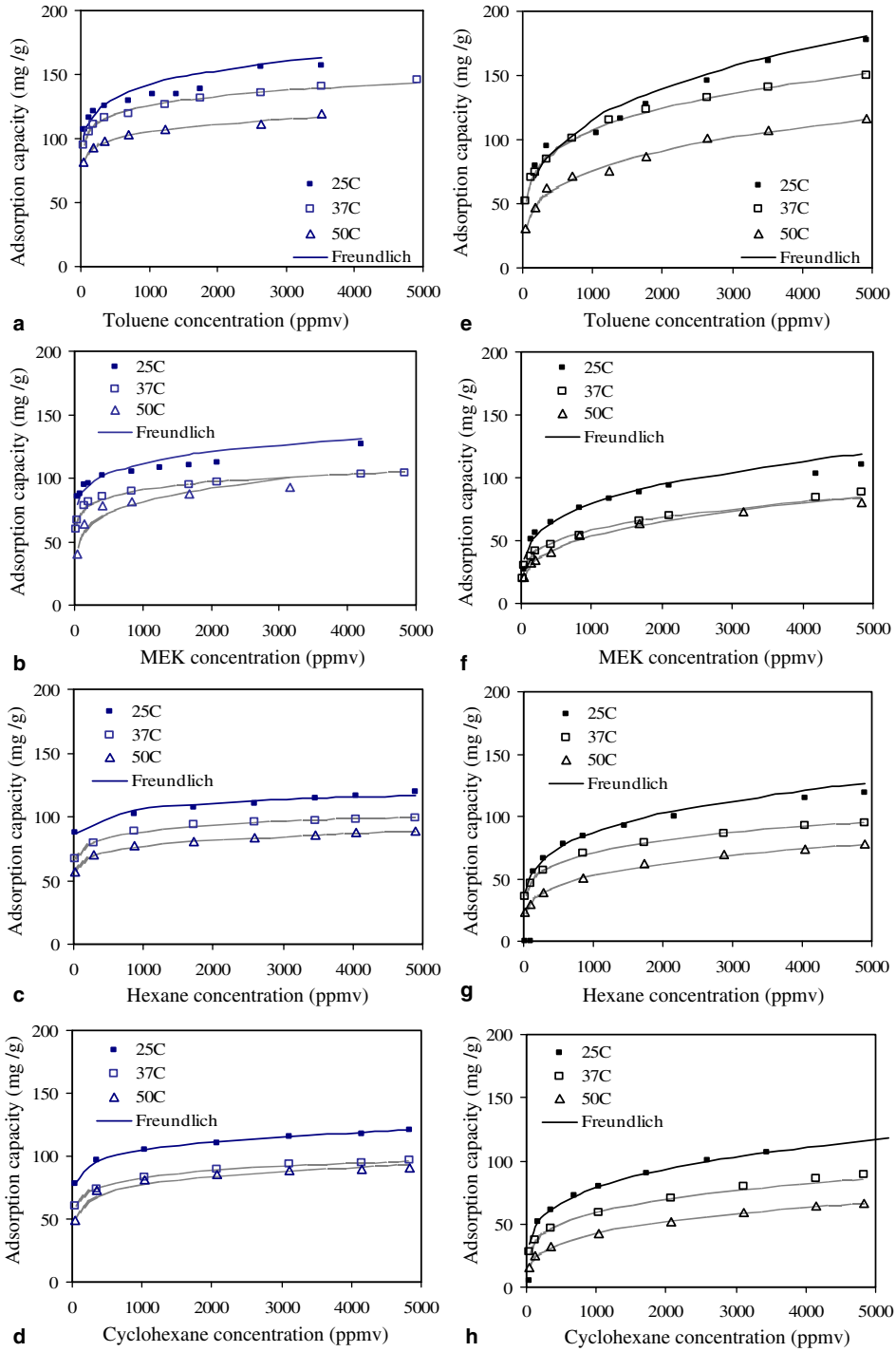

Fig. 2. Experimental data (symbols) and Freundlich isotherms (lines) of organic vapor adsorption on samples EA95 (a–d) and CVD80 (e–h).

Fig. 4). The void spacing between the nanotube bundles (Fig. 4b) is probably too wide for organic vapors to condense until complete saturation ($p/p_0 \approx 1$) is achieved.

The minimum measured adsorption capacities of sample EA95 at 30–40 ppmv were ≈40% of the maximum adsorption capacities at $p/p_0 \approx 0.9$, which shows that some SWNTs could have high potential for adsorption from vapor concentrations <30 ppmv.

3.3. Isotherm modeling

The Freundlich equation, which is widely used for describing the adsorption behavior of organic molecules on activated carbon [30], was fitted to the isotherm data (ppmv ⩽ 5000 and 25, 37 and 50 °C). Calculated parameters for the Freundlich equation and the percent relative error between measured and predicted values are

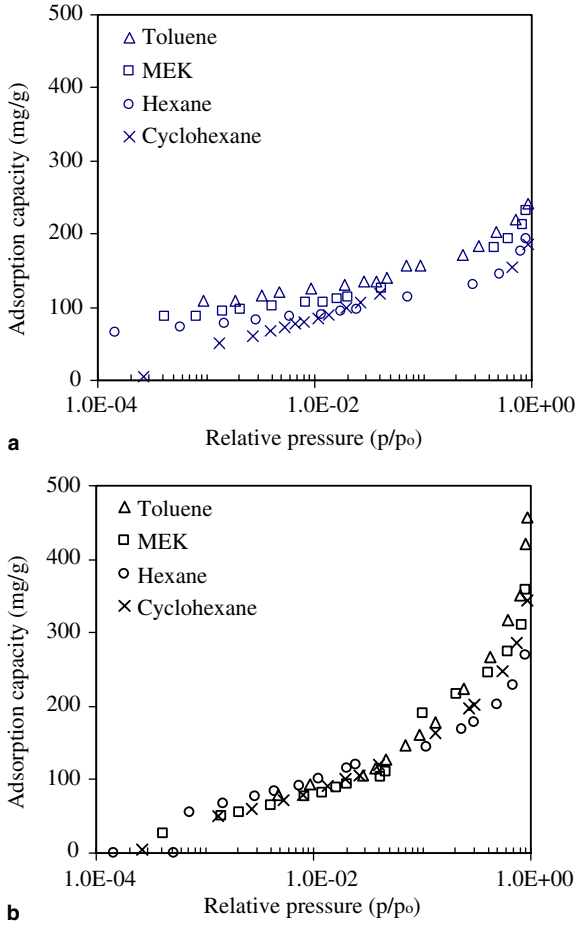

Fig. 3. Experimental data of organic vapor adsorption on samples (a) EA95 and (b) CVD80 at 25 °C. Isotherms calculated from Freundlich equation are not presented here for clarity.

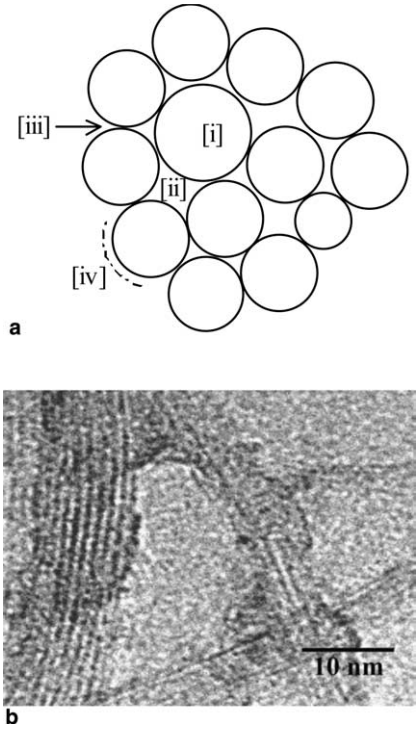

Fig. 4. (a) Cross-section of a SWNT bundle describing possible adsorption sites and (b) high resolution transmission electron image of sample EA95 [25]. Notice that multilayer adsorption on site [iv] would fill the void space between the SWNT bundles.

presented in Table 4. The predicted values are shown as lines in Fig. 2. The percent relative error between experimental and predicted values for SWNT samples ranged from 1% to 7%. Data fitting to the entire isotherm ($1 \times 10^{-4} < p/p_0 < 0.95$ at 25 °C, Fig. 3) projected slightly higher errors between 3% and 8%.

The experimental data were also fitted to other common isotherm models such as, Langmuir equation [31] and DR equation [32]. Although these isotherm

Table 3
Range of adsorption capacities of SWNTs at 25 °C

Adsorbent	Adsorbate	Minimum adsorption capacity[a]		Maximum adsorption capacities (at specified p/p_0 values)		
		ppmv	Adsorption capacity (mg/g)	p/p_0	Adsorption capacity (mg/g)	Total pore volume[b] (cm^3/g)
EA95	Toluene	35	108	0.94	242	0.28
	MEK	42	86	0.90	232	0.30
	Hexane	29	89	0.88	194	0.29
	Cyclohexane	35	78	0.93	198	0.25
					216 ± 24[c]	0.28 ± 0.02[c]
CVD80	Toluene	176[d]	80	0.94	456	0.52
	MEK	42	27	0.90	358	0.46
	Hexane	144[d]	56	0.88	269	0.40
	Cyclohexane	35	5	0.93	343	0.43
					356 ± 77[c]	0.45 ± 0.05[c]

[a] Minimum adsorption capacity was measured at 30–40 ppmv vapor concentrations. Lower concentrations were not generated due to their close proximity to concentration of organic vapors (<0.5 ppmv) already present in UHP N_2 carrier gas.
[b] Total pore volume = adsorption capacity (g/g)/bulk liquid density of vapor (g/cm^3).
[c] Mean ± standard deviation.
[d] Adsorption was not detected for concentrations below these values.

Table 4
Freundlich constants for adsorption of organic vapors on SWNTs[a]

Adsorbent	Adsorbate	25 °C			37 °C			50 °C		
		k	n	Error (%)[b]	k	n	Error (%)[b]	k	n	Error (%)[b]
EA95	Toluene	65.7	8.9	4.3	70.6	11.9	0.9	26.9	7.8	1.5
	MEK	52.6	9.2	4.4	47.0	10.9	1.8	22.9	5.4	2.1
	Hexane	71.5	17.5	1.9	29.6	11.1	1.8	50.8	13.4	1.4
	Cyclohexane	57.6	11.6	0.5	48.3	10.5	1.4	44.8	9.8	1.7
				2.8 ± 1.9[c]			1.6 ± 0.4[c]			1.7 ± 0.3[c]
CVD80	Toluene	16.5	3.6	7.8	24.4	4.7	1.2	11.9	3.7	2.8
	MEK	13.4	3.9	6.7	12.1	4.4	4.6	7.4	3.5	3.1
	Hexane	17.8	4.3	1.5	19.4	5.3	0.9	9.9	4.1	2.0
	Cyclohexane	14.6	4.1	0.7	11.9	4.3	2.2	6.0	3.5	2.2
				4.2 ± 3.6[c]			2.3 ± 1.7[c]			2.4 ± 0.5[c]

[a] Freundlich equation is $x/m = kC^{1/n}$, where x is mass adsorbed at equilibrium (mg), m is mass of the adsorbent (g), C is vapor concentration (ppmv), and k and n are constants [30]. The calculated values of k and n are applicable only to the isotherm data $\leqslant$5000 ppmv (Fig. 2). The adsorption capacities predicted from these constants are presented as lines in Fig. 2.

[b] Error (%) $= \frac{1}{N_I}\sum_{i=1}^{N_I}\left(\frac{1}{N_{T,i}}\sum_{j=1}^{N_{T,i}}\left[\frac{|q_{mod,j}-q_{expt,j}|}{q_{expt,j}}\times 100\right]\right)$, where N_I is the number of isotherms, $N_{T,i}$ is the number of points in each isotherm, and $q_{mod,j}$ and $q_{expt,j}$ are fitted and measured adsorption capacities, $N_{T,i}$ is the number of data points in an isotherms.

[c] Mean ± standard deviation.

equations have predictive capabilities, they appeared less compatible, with large errors (up to 29%) between the measured and modeled values (Table 5 and Fig. 5).

The isotherm modeling also provided insights into the heterogeneous nature of nanotubes as adsorbents. Increasing the sample temperature reduced the relative error between experimental and predicted data (Table 4) irrespective of isotherm model used (Fig. 5), which is a typical behavior of heterogeneous adsorbents [29]. Heterogeneity is a complex, more realistic, non-ideal behavior of an adsorbent. Heterogeneous adsorbents have several different types of adsorption sites with different activation energies. The adsorption sites with highest activation energy are filled first, and as the vapor pressure is increased the sites with lower energies are consumed [29]. Increasing the temperature allows adsorption to occur predominantly on sites with higher activation energy (which lowers the overall adsorption capacity), which makes them appear less heterogeneous and, therefore, more compatible with the assumptions used to develop selected isotherm models. Additionally, the argument that nanotubes are heterogeneous adsorbents is also supported by the fact that of the three isotherm equations tested, only the Freundlich equation seemed appropriate for describing the adsorption behavior on nanotubes. This is because the Freundlich equation assumes the

Table 5
Langmuir and DR constants for adsorption of organic vapors on SWNTs at 25 °C

Adsorbent	Adsorbate	Langmuir[a]			DR[b]		
		n_m (mol/g)	b	Error (%)	W_0[c] (cm^3/g)	βE_0 (kJ/mol)	Error (%)
EA95	Toluene	0.0017	0.0436	11.2	0.21	22.4	8.2
	MEK	0.0018	0.0034	26.0	0.19	22.4	8.1
	Hexane	0.0010	0.092	6.0	0.15	31.6	4.0
	Cyclohexane	0.0013	0.072	5.4	0.16	31.6	2.9
				12.2 ± 9.6[d]			5.8 ± 2.8[d]
CVD80	Toluene	0.0016	0.0063	11.6	0.25	11.9	14.9
	MEK	0.0014	0.0076	15.4	0.21	14.1	11.9
	Hexane	0.0011	0.0087	7.6	0.22	18.2	1.8
	Cyclohexane	0.0012	0.0052	29.0	0.33	11.2	23.0
				15.9 ± 9.3[d]			12.9 ± 8.8[d]

[a] Langmuir equation is $n/n_m = bC/(1 + bC)$, where n is adsorption capacity (moles/g), n_m is the monolayer adsorption capacity (moles/g), C is vapor concentration (ppmv) and b is constant [31].

[b] DR equation is $W/W_0 = \exp[-(A/\beta E_0)]$, where W is adsorption capacity (cm^3/g), W_0 is the micropore volume (cm^3/g), A is differential molar work (J/mol), β is similarity coefficient and E_0 is characteristic energy (J/mol) [32].

[c] W_0 values for sample EA95 and CVD80 were larger than those determined by N_2 adsorption (Table 1).

[d] Mean ± standard deviation.

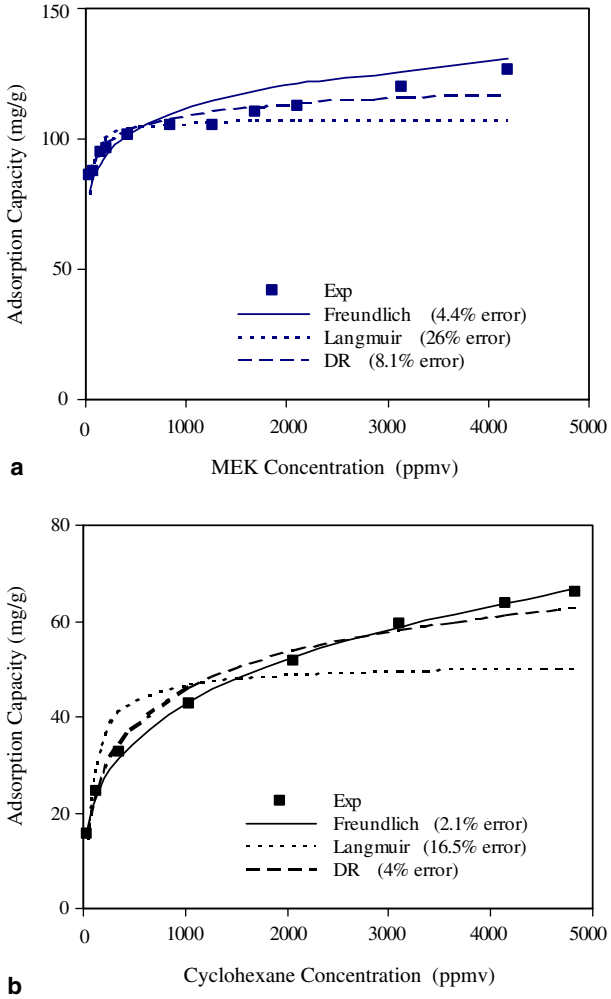

Fig. 5. Comparison of adsorption isotherm models with experimental results for (a) MEK adsorption on sample EA95 at 25 °C and (b) cyclohexane adsorption on sample CVD80 at 50 °C.

adsorbent surface to be heterogeneous, as opposed to the Langmuir equation that assumes a homogeneous adsorbent (i.e. same activation energy for all sites) and the DR equation, which best describes adsorption due to micropore filling mechanisms. The heterogeneity of SWNTs is a result of multiple adsorption sites on nanotube bundles (Fig. 4a), which have different geometries and thus different activation energies for adsorption. The contributions of these multiple sites to overall adsorption could differ from sample to sample depending on the percentage of open-ended nanotubes in a sample, surface defects and chemical functional groups.

3.4. Isosteric heat of adsorption

The isosteric heat of adsorption (ΔH_s) characterizes the activation energy for sorption and, thus, denotes the strength of adsorbate–adsorbent interaction [29]. Quantification of ΔH_s values is important for kinetic studies because the heat released upon adsorption is partly absorbed by the adsorbent, which raises the adsorbent's temperature and thus slows the rate of adsorption as equilibrium is approached [29].

ΔH_s values for the adsorption of organic vapors onto samples EA95 and CVD80 were calculated from the adsorption data obtained at multiple temperatures (Figs. 2 and 3) using the Gibbs–Helmholtz equation [33] for constant adsorbed phase concentrations of 50, 80 and 100 mg/g (Table 6). ΔH_s values were 1–4 times the heats of vaporization for each respective vapor (Table 1), which is typical for physical adsorption [29]. The general trend of ΔH_s for both adsorbents was hexane (highest) > cyclohexane > toluene > MEK (lowest), which is the opposite trend for the dipole moments for the organic vapors. Significantly lower ΔH_s values for MEK, which had the highest dipole moment of 1.1×10^{-29} C m of the organic vapors tested here, suggests a non-polar surface for the adsorbents.

The dependence of the ΔH_s values on loading is an indication that adsorption is occurring on different types of sites. The ΔH_s values for sample EA95 were greater than the values for sample CVD80 for all organic vapors

Table 6
Heat of adsorption of organic vapors on SWNTs[a]

Adsorbent	Adsorbate	ΔH_s (kJ/mol)		
		q = 50 mg/g	q = 80 mg/g	q = 100 mg/g
EA95	Toluene	n.a.[b]	95	73.5
	MEK	n.a.[b]	99.8	64.5
	Hexane	256.3	174.4	129.0
	Cyclohexane	158.2	112.8	84.8
CVD80	Toluene	n.a.[b]	68.6	38.3
	MEK	n.a.[b]	43.0	22.6
	Hexane	69.5	68.5	58.6
	Cyclohexane	79.5	71.0	65.4

[a] Heat of adsorption was determined by the Gibbs–Helmholtz equation, $\left(\frac{\partial \ln p}{\partial T}\right)_q = \frac{-\Delta H_s}{RT^2}$, where p is the vapor pressure (atm), T is temperature (K), q is adsorption capacity (mg/g) and R is universal gas constant (J/mol K) [33].

[b] n.a. = Not available.

at same coverage. This result indicates that the organic vapors interacted more strongly with the EA95 sample than the CVD80 sample. This result also suggests that different adsorption sites were populated on the two different samples at the same loading, especially when comparing results at a loading of 50 mg/g. The present data set is insufficient to determine activation energies associated with each adsorption sites of the two samples. However, as previously mentioned, adsorption proceeds from sites of high activation energy to low activation energy; thus, for sample EA95 exceptionally high heats of adsorption at a loading of 50 mg/g, which are obtained at $p/p_0 < 10^{-2}$ (mainly internal adsorption), are most likely the activation energies for organic adsorption in sites [i] and [ii] (Fig. 4a). For sample CVD80, however, such a distinction could not be made, as ΔH_s for this sample did not exhibit appreciable dependence on surface loading.

4. Summary and conclusions

In this study gravimetric methods were used to determine the equilibrium adsorption capacities of toluene, methyl ethyl ketone (MEK), hexane and cyclohexane on commercially available, purified, electric arc, and HiPco CVD manufactured single-walled carbon nanotube (SWNTs) samples. The isotherms of both samples followed certain characteristics of type I and type II adsorption isotherms, even though the samples were mainly mesoporous with only 10–40% of their total pore volume in micropores. The relative adsorption capacities of both samples was in the order of toluene (maximum) > MEK > hexane > cyclohexane (minimum), which did not follow any particular molecular property. It is speculated that until $p/p_0 \approx 10^{-2}$ organic vapors saturate the internal volume of nanotubes and at $p/p_0 > 10^{-2}$ adsorption occurs only on the outer surface of the bundles (i.e. in the void spacing between the bundles). The Freundlich isotherm equation fitted the experimental data more closely than the Langmuir or DR equations, due to the heterogeneity of SWNT adsorption sites. The heats of adsorption of organic vapors of the two samples were 1–4 times their heats of vaporization, which is typical for physical adsorption.

References

[1] Fujiwara A, Ishji K, Suematsu H, Kataura H, et al. Gas adsorption in the inside and outside of single-walled carbon nanotubes. Chem Phys Lett 2001;336(3):205–11.

[2] Mawhinney DB, Naumenko V, Kuznetsova A, Yates Jr JT, et al. Surface defect site density on single-walled carbon nanotubes by titration. Chem Phys Lett 2000;324(1):213–6.

[3] Dresselhaus MS, Dresselhaus G, Avouris P. Carbon nanotubes: synthesis, structure, properties and applications. Top Appl Phys 2000;80:393–4.

[4] Long RQ, Yang RT. Carbon nanotubes as superior sorbents for nitrogen oxides. Ind Eng Chem Res 2001;40:4288–91.

[5] Cinke M, Li J, Chen B, Cassell A, et al. Pore structure of raw and purified HiPco single-walled carbon nanotubes. Chem Phys Lett 2002;365:69–74.

[6] Yin YF, Mays T, McEnanaey B. Adsorption of nitrogen in carbon nanotube arrays. Langmuir 1999;15:8714–8.

[7] Long RQ, Yang RT. Carbon nanotubes as superior sorbents for dioxin removal. J Am Chem Soc 2001;123(9):2058–9.

[8] Peng X, Li Y, Luan Z, Di Z, et al. Adsorption of 1,2-dichlorobenzene from water to carbon nanotubes. Chem Phys Lett 2003;376:154–8.

[9] Li Y, Wang S, Zhang W, Wei J, et al. Adsorption of fluoride from water by aligned carbon nanotubes. Mat Res Bull 2003;38:469–476.

[10] Liu C, Fan YY, Liu M, Cong HT, et al. Hydrogen storage in single-walled carbon nanotubes at room temperature. Science 1999;286(5442):1127–9.

[11] Varghese OK, Kichambre PD, Gong D, Ong KG, et al. Gas sensing characteristics of multi-wall carbon nanotubes. Sensors Actuators B 2001;81(1):32–41.

[12] Kong J, Franklin NR, Zhou C, Chapline MG, et al. Nanotube molecular wires as chemical sensors. Science 2000;287:622–5.

[13] Talapatra S, Zambano AZ, Weber SE, Migone AD. Gases do not adsorb on the interstitial channels of close-ended single-walled carbon nanotube bundles. Phys Rev Lett 2000;85(1):138–41.

[14] Duren T, Keil FJ. Molecular modeling of adsorption in carbon nanotubes. Chem Eng Technol 2001;24:698–702.

[15] Mao Z, Lee KH, Sinnott SB. Nanotubes as membranes: predictions of atomistic simulations. Energeia 2003;14(2):1–4.

[16] Mao Z, Sinnott SB. Separation of organic molecular mixture in carbon nanotube and bundles: molecular dynamics simulations. J Phys Chem B 2001;105:6916–24.

[17] Eswaramoorthy M, Sen R, Rao CNR. A study of micropores in single-wall carbon nanotubes by the adsorption of gases and vapors. Chem Phys Lett 1999;304:207–10.

[18] Talapatra S, Migone AD. Adsorption of methane on bundles of closed-ended single-wall carbon nanotubes. Phys Rev B 2002;65(4):045416.

[19] Bittner EW, Smith MR, Bockrath BC. Characterization of surfaces of single-walled carbon nanotubes using alcohols and hydrocarbons: a pulse adsorption technique. Carbon 2003;41(6):1231–9.

[20] Weast RC. CRC handbook of chemistry and physics. Boca Raton, FL: CRC Press; 1984. p. C154–321.

[21] Reid RC, Prausnitz JM, Poling BE. The properties of gases and liquids. New York: Wiley; 1984. p. 656–732.

[22] ChemSketch. Ver. 4.0. Advanced Chemistry Development Inc.: Toronto, ON; 1999.

[23] Nikolaev P, Bronikowski MJ, Bradley RK, Rohmund F, et al. Gas-phased catalytic growth of singe-walled carbon nanotubes from carbon monoxide. Chem Phys Lett 1999;313(1):91–7.

[24] Bronikowski MJ, Willis PA, Colbert DT, Smith KA, et al. Gas-phase production of carbon single-walled nanotubes from carbon monoxide via HiPco process: a parametric study. J Vac Sci Technol A 2001;19(4):1800–5.

[25] Agnihotri S, Rostam-Abadi M, Rood MJ. Temporal changes in nitrogen adsorption properties of single-walled carbon nanotubes. Carbon 2004;42(12):2699–710.

[26] Rinzler AG, Liu J, Dai H, Nikolev P, et al. Large-scale purification of single-wall carbon nanotubes: process, product, and characterization. Appl Phys A 1998;67(1):29–37.

[27] Agnihotri S, Mota PB, Rostam-Abadi M, Rood MJ. Structural characterization of single-walled carbon nanotubes bundles by experiment and molecular simulation. Langmuir 2005;21(3):896–904.

[28] Brunauer S, Deming LS, Deming WE, Teller EJ. On a theory of the van der Waals adsorption of gases. J Am Chem Soc 1940;62(7):1723–32.
[29] Do DD. Adsorption analysis: equilibria and kinetics. London: Imperial College Press; 1998.
[30] Freundlich H. Of the adsorption of gases. Section II. Kinetics and energetics of gas adsorption. Introductory paper to Section II. Trans Farad Soc 1932;28(1):195–201.
[31] Langmuir I. The adsorption of gases on plane surfaces of glass, mica and platinum. J Am Chem Soc 1918;40(9):1361–403.
[32] Dubinin MM. Fundamentals of the theory of adsorption in micropores of carbon adsorbents: characteristics of their adsorption properties and microporous structure. Carbon 1989;27(3):457–67.
[33] Ruthven DM. Principles of adsorption and adsorption processes. Wiley Interscience Publication; 1984. p. 62–5.